

# A computational model of radiofrequency ablation in the stomach, an emerging therapy for gastric dysrhythmias

Matthew Savage, Recep Avci, *Member, IEEE*, Zahra Aghababaie, Ashton Matthee, Faraz Chamani,  
Punit Prakash, *Member, IEEE*, Leo K. Cheng, and Timothy R. Angeli-Gordon, *Member, IEEE*

**Abstract**— Gastric ablation has recently emerged as a promising potential therapy for bioelectrical dysrhythmias that underpin many gastrointestinal disorders. Despite similarities to well-developed cardiac ablation, gastric ablation is in early development and has thus far been limited to temperature-controlled, non-irrigated settings. A computational model of gastric ablation is needed to enable *in silico* testing and optimization of ablation parameters and techniques. In this study, we developed a computational model of radio-frequency (RF) gastric ablation. Model parameters and boundary conditions were established based on the current *in vivo* experimental application of serosal gastric ablation with a non-irrigated RF catheter. The Pennes bioheat transfer equation was used to model the thermal component of RF ablation, and Laplace's equation was used to model the Joule heating component. Tissue, blood, and catheter parameters were obtained from literature. The performance of the model was compared to previously established experimental values of temperature measured from various distances from the catheter tip. The model produced temperature estimations that were within 6% of the maximum experimental temperature at 2.5 mm from the catheter, and within 13% of the maximum temperature change at 4.7 mm. This model now provides a computational basis through which to conduct *in silico* testing of gastric ablation, and can be usefully applied to optimize gastric ablation parameters. In future, the model can be expanded to include irrigation of the catheter tip and power-controlled RF settings.

**Clinical Relevance**— This work presents a computational model of gastric ablation that can now guide the *in silico* development of effective ablation parameters and therapeutic strategies, expanding the breadth of this promising therapy.

## I. INTRODUCTION

Rhythmic bioelectrical 'slow waves' are a critical controlling mechanism of gastrointestinal (GI) motility, initiated and propagated by interstitial cells of Cajal (ICC) [1]. Similar to the heart, slow wave activity is highly organized in the healthy stomach, and abnormal electrical dysrhythmias have been associated with several GI motility disorders including gastroparesis, chronic unexplained nausea and vomiting, and dyspepsia [2]–[4]. Despite similarities to bioelectrical cardiac arrhythmias, which underpin an entire

cardiac therapy industry, no proven therapies currently exist for correcting dysrhythmias in the stomach.

Ablation has been established as a successful treatment for cardiac arrhythmias for many decades [5], including recent data demonstrating that ablation out-performs drug therapy in patients with paroxysmal atrial fibrillation [6]. Ablation has only recently been translated to the stomach, where initial experimental evidence now shows that radiofrequency (RF) ablation of gastric smooth muscle and ICC can create an electrical barrier to slow wave conduction and could likely be used to eliminate dysrhythmic gastric conduction mechanisms [7], [8].

Gastric ablation now offers a promising potential therapeutic option for GI disorders, where few options currently exist [9]. *In silico*, computational modeling is needed to define the effects of ablation in stomach tissue. Computational models of ablation exist for other organs (*e.g.*, liver [10], [11] and heart [12]), but a dedicated gastric ablation model is needed to accurately inform parameter optimization and new ablation strategies.

## II. MODEL DEVELOPMENT

### A. Model Structure

A model of gastric ablation was structured as shown in Fig. 1, based on recent porcine *in vivo* experiments that demonstrated the feasibility and efficacy of the technique [7], as well as preliminary temperature data [13]. A finite difference model was implemented using MATLAB R2020a (MathWorks, Natick, MA, USA) to estimate the temperature distribution and lesion size based on prescribed ablation temperature and duration. The model was implemented in 3-dimensions using cuboid simulation cells. A catheter with a 3.5 mm diameter was applied to the serosal surface assuming no tissue deformation, modeled as a round rod with a flat end that was assumed to be in perfect contact with the tissue. The catheter was surrounded by a 1 mm layer of surface fluid. The simulations were performed across a domain size of 20 mm wide x 20 mm long x 10 mm deep, using spatial step sizes of 0.2-0.5 mm and temporal step sizes of 0.05-10 ms, to empirically compare the accuracy and computational efficiency at different step sizes.

This research was supported by funding from the Health Research Council (HRC) of New Zealand, and the Royal Society Te Apārangi. T. R. Angeli-Gordon was supported by a Rutherford Discovery Fellowship from the Royal Society Te Apārangi. M. Savage was supported by a scholarship from the Medical Technology Centre of Research Excellence (MedTech CoRE), New Zealand.

M. Savage, R. Avci, Z. Aghababaie, A. Matthee, L. K. Cheng, and T. R. Angeli-Gordon are with the Auckland Bioengineering Institute, University of Auckland, Auckland, New Zealand. (Corresponding author: T. R. Angeli-Gordon; phone: +64-9-373-7999; e-mail: [t.angeli@auckland.ac.nz](mailto:t.angeli@auckland.ac.nz)).

P. Prakash and F. Chamani are with the Electrical and Computer Engineering Dept., Kansas State University, Manhattan, KS 66506, USA.

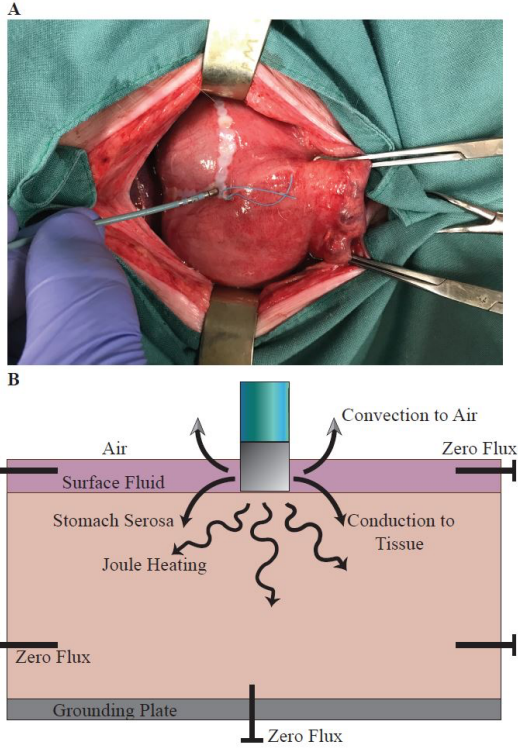


Figure 1. A) Photo of the ablation catheter positioned on the gastric serosa in an *in vivo* application, where RF ablation was performed with a Stokert 70 RF generator at a working frequency of 500 kHz (Biosense Webster, Irvine, CA, USA) [7]. B) Schematic representation of gastric ablation model. The catheter was modeled as being in direct contact with the serosal surface of the stomach, with a thin (1 mm) layer of surface fluid around the catheter, consistent with *in vivo* applications of serosal ablation [7]. Convective heat loss was set as the upper boundary condition, which is open to air in the *in vivo* setup, and zero flux was set for all other boundaries.

### B. Mathematical Foundation and Implementation

The RF ablation model was based on a time domain analysis of a coupled electric-thermal problem. Pennes bioheat equation was used to thermally model the spatial distribution of temperature in the tissue for a given density, specific heat, thermal conductivity, rate of perfusion and rate of heating [14]:

$$\rho_t c_t \frac{\partial T}{\partial t} = \nabla \cdot k_t \nabla T + Q_J - Q_p \quad (1)$$

where  $\rho_t$  is the tissue density,  $c_t$  is the specific heat of the tissue,  $T$  is temperature of the tissue,  $t$  is time,  $k_t$  is the thermal conductivity of the tissue,  $Q_J$  corresponds to the distributed heat source due to the electric field (also known as ‘Joule heating’), and  $Q_p$  is the perfusion heat loss.

The Joule heating from the electric field is given by [15]:

$$Q_J = \sigma |\mathbf{E}|^2 = \sigma |-\nabla V|^2 \quad (2)$$

where  $\sigma$  is electrical conductivity of the tissue,  $\mathbf{E}$  is the electric field, and  $V$  is the potential field. Laplace’s equation was used to determine the potential field across the tissue block [14]:

$$\nabla \cdot [\sigma(T) \cdot \nabla V] = 0 \quad (3)$$

When applied to a Taylor series expansion in 3-dimensions, the solution of  $V$  was:

$$V(x, y, z) = \frac{1}{6}(V(x+h, y, z) + V(x-h, y, z) + V(x, y+h, z) + V(x, y-h, z) + V(x, y, z+h) + V(x, y, z-h)) \quad (4)$$

where  $V(x, y, z)$  is the potential at a point  $(x, y, z)$ , and  $h$  is a small step in distance. The potential at any point can be approximated by the average potential of the surrounding points. Equation (4) can be iteratively solved for the following boundary conditions:

$$V_p = V_s \quad (5)$$

$$V_n = 0 \quad (6)$$

where  $V_p$  is the catheter voltage,  $V_s$  is the source voltage, and  $V_n$  is the voltage at the grounding plate. A maximum of 600 iterations were performed to refine the voltage to an error of less than 0.01 V.

The amount of heat loss due to the blood perfusion was calculated using [14],

$$Q_p = \rho_b \omega_b c_b (T - T_b) \quad (7)$$

where  $\rho_b$  is the density of blood,  $\omega_b$  is the rate of perfusion,  $c_b$  is the specific heat of blood, and  $T_b$  is the arterial blood temperature.

The heat distribution also depends on where the cell was located relative to each boundary in the model (Fig. 1). A convection boundary condition was applied to the cells on the gastric serosa exposure to the fluid, and to the fluid exposure to the air, which were calculated by [10]:

$$k_t \nabla T|_{surface} = h_A (T_{env} - T) \quad (8)$$

where  $h_A$  is the convective heat transfer coefficient of the surface area, and  $T_{env}$  is the environmental temperature.  $T_{env}$  for the surface fluid was modeled at 33 °C based on the baseline catheter tip temperature during *in vivo* gastric ablations [13], while  $T_{env}$  for air was modeled as typical room temperature of 25 °C.

Similarly, conductive heat due to the catheter temperature was modeled using:

$$k_t \nabla T|_{catheter} = \frac{K \Delta T}{L} \quad (9)$$

where  $K$  is the thermal conductivity of the catheter material,  $\Delta T$  is the temperature difference,  $A$  is the surface area that the heat passes through, and  $L$  is the distance travelled. The catheter temperature was set to 70 °C for the validation here, with an on/off controller to match experimental temperatures.

### C. Parameter Values

The parameters used in the model are shown in Table 1. These data were obtained from literature and/or publicly available online data repositories, with references included in Table 1.

## III. MODEL VALIDATION

A spatial step size ( $dx$ ) of 0.2 mm and a temporal step size ( $dt$ ) of 0.5 ms were empirically found to provide a suitable balance of accuracy versus computational time, and were thereby used for the results reported here. The model was compared against experimental data from custom temperature probes applied during *in vivo* RF serosal ablation in the

porcine stomach [13]. The maximum tissue temperatures calculated by the model were within 15% of experimental *in vivo* temperature values across the entire modeled tissue area (Fig. 2A). The model closely matched experimental data in regions near the catheter tip, including similar maximum temperature over-shoot beyond the 70 °C setting, but the accuracy of the model decreased with distance from the catheter (Fig. 2A). For example, at 2.5 mm from the catheter tip, the maximum temperature was comparable between *in vivo* data and our new *in silico* model, being within 6% of the maximum temperature reached during a 10 s ablation, but at 4.7 mm from the catheter tip that difference grew to the model prediction being 13% lower maximum temperature than the experimental data (Fig. 2A).

TABLE I. PARAMETERS APPLIED IN GASTRIC ABLATION MODEL

Parameter		Value	Reference
Gastric tissue	Density ( $\text{kg}\cdot\text{m}^{-3}$ )	1088	[16]
	Specific heat ( $\text{J}\cdot\text{kg}^{-1}\cdot\text{°C}^{-1}$ )	3690 <sup>a</sup>	[16]
	Electrical conductance ( $\text{S}\cdot\text{m}^{-1}$ )	1.025 <sup>b</sup>	[16]
	Thermal conductivity ( $\text{W}\cdot\text{m}^{-1}\cdot\text{°C}^{-1}$ )	0.53 <sup>c</sup>	[16]
Catheter	Thermal conductivity ( $\text{W}\cdot\text{m}^{-1}\cdot\text{°C}^{-1}$ )	71.6 <sup>d</sup>	[17]
	Diameter (mm)	3.5	-
Air convection ( $\text{W}\cdot\text{m}^{-2}\cdot\text{°C}^{-1}$ )		10.0	Est.
Room temperature (°C)		25.0	Est.
Body temperature (°C)		33.0	[13]
Blood perfusion ( $\text{s}^{-1}$ )		0.0064	[18]
Spatial step sizes, $dx$ (mm)		0.2 – 0.5	-
Temporal step sizes, $dt$ (ms)		0.05 – 10	-

a. Variable with temperature, increasing at  $28.9 \text{ J}\cdot\text{kg}^{-1}\cdot\text{°C}^{-1}$  between  $63.5 - 83.4 \text{ °C}$ .

b. Variable with temperature, increasing at  $1.5 \text{ S}\cdot\text{m}^{-1}\cdot\text{°C}^{-1}$ .

c. Variable with temperature, increasing at  $0.0008 \text{ W}\cdot\text{m}^{-1}\cdot\text{°C}^{-1}$ .

d. The catheter tip was a platinum alloy, so the conductivity for platinum was used.

Fig. 2B and 2C show the maximum temperature profile and current density field, respectively, as a 2D cross-section of the 3D model. These 2d cross-sections accurately reflect the 3D results because the model is symmetrical around the rotational axis due to the assumption of tissue homogeneity through the domain. These data demonstrate that the model achieved a reasonably sized and shaped thermal and current distribution, compared to ablation models developed for other organs [10], [12], and the current distribution was comparable to preliminary histological results of gastric ablation [7].

#### IV. DISCUSSION

In this study, we developed a novel computational model of RF ablation in the stomach. Our model was structured to match the setup of recently developed *in vivo* gastric ablation [7], and the results demonstrated that our model is accurate to within 15% of experimental *in vivo* temperature data [13]. This gastric ablation model now offers an *in silico* tool for

investigating and optimizing parameters for gastric ablation. Gastric ablation offers a promising therapeutic approach for GI disorders, where electrical dysrhythmias in the stomach could be disrupted by ablation, but substantial additional work is required to ultimately determine clinical effectiveness.

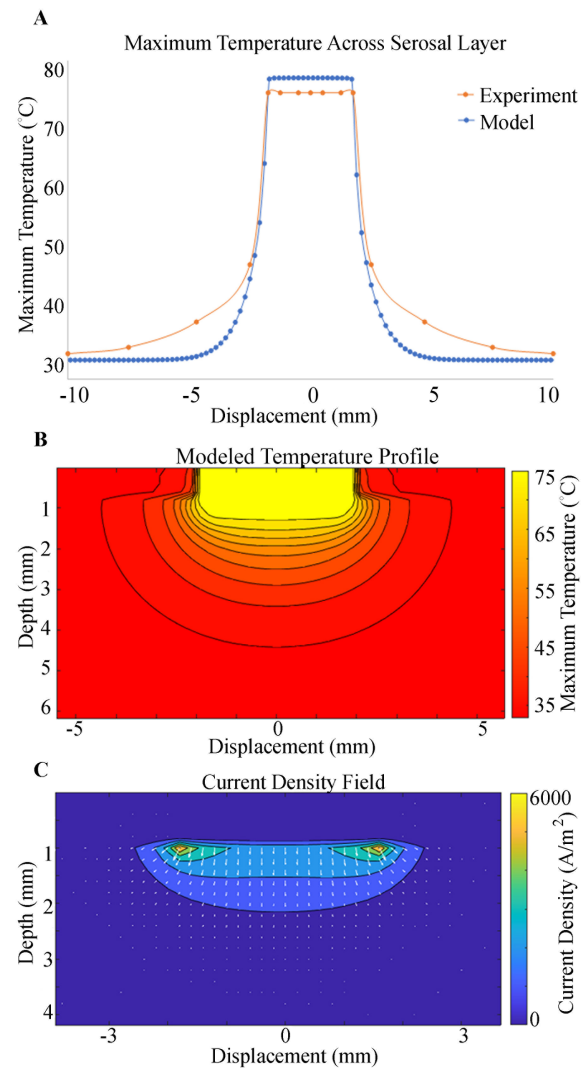


Figure 2. Gastric RF ablation model results. A) Comparison of maximum serosal temperature predicted by the model (blue) versus measured during *in vivo* experiments (orange, [13]), during a gastric ablation performed at 70 °C for 10 s duration. B) Corresponding modeled temperature profile, and C) current density field, shown as a 2D cross-section of the 3D model, which was symmetrical about the rotational axis. The layer from 0-1 mm of depth represents the surface fluid layer. The model domain was 20x20x10 mm; images here have been cropped to highlight the region of interest.

Our model demonstrated a steeper decay of tissue temperature versus distance from the catheter, compared to experimental data, *i.e.*, our model has a higher loss of thermal energy at distances away from the catheter tip. The cross-sectional temperature profile demonstrated that the surface fluid layer was notably lower in temperature than the gastric tissue, effectively carrying heat away from the tissue via convective loss to the air, as expected (Fig. 2B). However, this convective heat loss, or the loss due to blood perfusion

through the gastric tissue, could be over-estimated in our current model, causing the decreased temperature compared to experimental data (Fig. 2A). In future, the surface fluid layer and blood perfusion could be optimized to better fit the experimental data, while still according with reasonable values based on the *in vivo* application (e.g., decrease surface fluid layer from 1 mm to 0.1-0.5 mm). Future expansion to include an estimate of the resultant lesion size would also be valuable, e.g., by using the Arrhenius equation [11], [19].

Our model was limited to temperature-controlled, non-irrigated, RF ablation from the serosal surface, which were parameters that were selected to match *in vivo* gastric ablation studies showing feasibility and efficacy of the technique for modulating bioelectrical activation of the stomach [7], [8], and temperature data for validation of the model [13]. Alternate ablation parameters like power-controlled RF or electroporation energy delivery, and irrigation of the catheter tip, offer potential for increased control of lesion size, depth, and shape, as has been demonstrated in cardiac ablation [20]–[22]. Gastric ablation from the mucosal surface could offer a minimally-invasive option for therapy in the future [7], and would complement minimally-invasive endoscopic electrical mapping diagnostics that are currently in development [23]. The small intestine exhibits complex electrical propagation, similar to gastric dysrhythmias [24], [25], where intestinal ablation may also be a useful future technique for modulation. Such parameters and ablation strategies could be usefully modeled in the future, based on the foundational RF gastric ablation model presented here.

## V. CONCLUSION

This study presents a computational model of RF gastric ablation that provides estimates of tissue temperature in 3-dimensions that are accurate to within 15% of published *in vivo* experimental data. The model supports a promising new field of gastric ablation for modulating electrical activation in the stomach and can now be applied to inform *in silico* investigation of alternative RF device geometries, energy-delivery parameters, methods of performing ablation, and strategies for therapy.

## REFERENCES

- [1] J. D. Huizinga and W. J. E. P. Lammers, "Gut peristalsis is governed by a multitude of cooperating mechanisms," *Am. J. Physiol. Gastrointest. Liver Physiol.*, vol. 296, no. 1, pp. G1-8, 2009.
- [2] G. O'Grady *et al.*, "Abnormal initiation and conduction of slow-wave activity in gastroparesis, defined by high-resolution electrical mapping," *Gastroenterology*, vol. 143, no. 3, pp. 589-598.e1-3, 2012.
- [3] T. R. Angeli *et al.*, "Loss of interstitial cells of Cajal and patterns of gastric dysrhythmia in patients with chronic unexplained nausea and vomiting," *Gastroenterology*, vol. 149, no. 1, pp. 56-66.e5, 2015.
- [4] A. A. Gharibans, T. P. Coleman, H. Mousa, and D. C. Kunkel, "Spatial patterns from high-resolution electrogastrography correlate with severity of symptoms in patients with functional dyspepsia and gastroparesis," *Clin. Gastroenterol. Hepatol.*, vol. 17, no. 13, pp. 2668-2677, 2019.
- [5] F. Morady, "Radio-frequency ablation as treatment for cardiac arrhythmias," *N. Engl. J. Med.*, vol. 340, pp. 534-544, 1999.
- [6] O. M. Wazni *et al.*, "Cryoballoon ablation as initial therapy for atrial fibrillation," *N. Engl. J. Med.*, vol. 384, no. 4, pp. 316-324, 2021.
- [7] Z. Aghababaie *et al.*, "Gastric ablation as a novel technique for modulating the bioelectrical control of the stomach," *Am. J. Physiol. Gastrointest. Liver Physiol.*, vol. 320, no. 4, pp. G573-G585, 2021.
- [8] Z. Aghababaie *et al.*, "Feasibility of high-resolution electrical mapping for characterizing conduction blocks created by gastric ablation," *Conf. Proc. IEEE. Eng. Med. Biol. Soc.*, vol. 1, pp. 170-173, 2019.
- [9] T. R. Angeli and G. O'Grady, "Challenges in defining, diagnosing, and treating diabetic gastroparesis," *J. Diabetes Complicat.*, vol. 32, no. 2, pp. 127-128, 2018.
- [10] F. Qin, K. Zhang, J. Zou, J. Sun, A. Zhang, and L. X. Xu, "A new model for RF ablation planning in clinic," *Conf. Proc. IEEE. Eng. Med. Biol. Soc.*, vol. 1, pp. 3232-3235, 2018.
- [11] M. Trujillo *et al.*, "How large is the periablational zone after radiofrequency and microwave ablation? Computer-based comparative study of two currently used clinical devices," *Int. J. Hyperth.*, vol. 37, no. 1, pp. 1131-1138, 2020.
- [12] A. Petras, M. Leoni, J. M. Guerra, J. Jansson, and L. Gerardo-Giorda, "A computational model of open-irrigated radiofrequency catheter ablation accounting for mechanical properties of the cardiac tissue," *Int. J. Numer. Meth. Biomed. Eng.*, vol. 35, no. 11, p. e3232, 2019.
- [13] M. Sayat *et al.*, "Transmural temperature monitoring to quantify thermal conduction and lesion formation during gastric ablation, an emerging therapy for gastric dysrhythmias," *Conf. Proc. IEEE. Eng. Med. Biol. Soc.*, vol. 1, pp. 5259-5262, 2020.
- [14] E. J. Berjano, "Theoretical modeling for radiofrequency ablation: State-of-the-art and challenges for the future," *Biomed. Eng. Online*, vol. 5, p. 24, 2006.
- [15] J. W. Strohbehn, "Temperature distributions from interstitial RF electrode hyperthermia systems: theoretical predictions," *Int. J. Radiat. Oncol. Biol. Phys.*, vol. 9, no. 11, pp. 1655-1667, 1983.
- [16] "Tissue properties database," *Foundation for Research on Information Technologies in Society (IT'IS)*. [Online]. Available: <https://itis.swiss/virtual-population/tissue-properties/database/>.
- [17] "Thermal conductivity of elements," *Angstrom Sciences*. [Online]. Available: <https://www.angstromsciences.com/thermal-conductivity-of-elements>.
- [18] I. A. Chang and U. D. Nguyen, "Thermal modeling of lesion growth with radiofrequency ablation devices," *Biomed. Eng. Online*, vol. 3, no. 1, p. 27, 2004.
- [19] W. C. Dewey, "Arrhenius relationships from the molecule and cell to the clinic," *Int. J. Hyperth.*, vol. 10, no. 4, p. 457-483, 1994.
- [20] H. H. Petersen, X. Chen, A. Pietersen, J. H. Svendsen, and S. Haunsø, "Tissue temperatures and lesion size during irrigated tip catheter radiofrequency ablation: an in vitro comparison of temperature-controlled irrigated tip ablation, power-controlled irrigated tip ablation, and standard temperature-controlled ablation," *Pacing Clin. Electrophysiol.*, vol. 23, no. 1, pp. 8-17, 2000.
- [21] A. Thiagalingam *et al.*, "Cooled needle catheter ablation creates deeper and wider lesions than irrigated tip catheter ablation," *J. Cardiovasc. Electrophysiol.*, vol. 16, no. 5, pp. 508-515, 2005.
- [22] S. J. Asirvatham, "Cardiac electroporation: The promise of the unknown," *J. Cardiovasc. Electrophysiol.*, vol. 29, pp. 652-654, 2018.
- [23] T. R. Angeli *et al.*, "High-resolution electrical mapping of porcine gastric slow-wave propagation from the mucosal surface," *Neurogastroenterol. Motil.*, vol. 29, no. 5, p. e13010, 2017.
- [24] T. R. Angeli, G. O'Grady, R. Vather, I. P. Bissett, and L. K. Cheng, "Intra-operative high-resolution mapping of slow wave propagation in the human jejunum: Feasibility and initial results," *Neurogastroenterol. Motil.*, p. e13310, 2018.
- [25] T. R. Angeli *et al.*, "Circumferential and functional re-entry of in vivo slow-wave activity in the porcine small intestine," *Neurogastroenterol. Motil.*, vol. 25, no. 5, pp. e304-314, 2013.